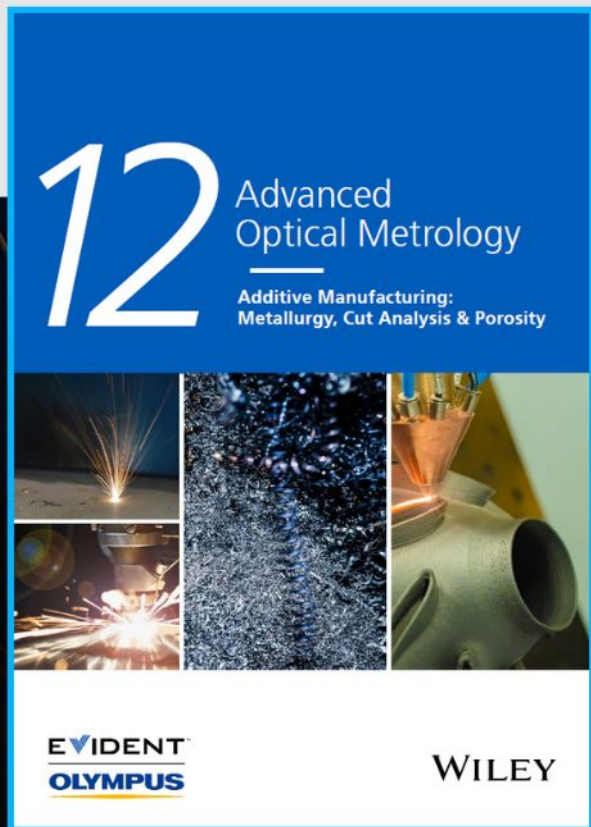




# Additive Manufacturing: Metallurgy, Cut Analysis & Porosity

The latest eBook from  
Advanced Optical Metrology.  
Download for free.



In industry, sector after sector is moving away from conventional production methods to additive manufacturing, a technology that has been recommended for substantial research investment.

Download the latest eBook to read about the applications, trends, opportunities, and challenges around this process, and how it has been adapted to different industrial sectors.

**EVIDENT™**  
**OLYMPUS**

**WILEY**

# Leveraging Bioinspired Structural Constraints for Tunable and Programmable Snapping Dynamics in High-Speed Soft Actuators

Jiao Wang, Tonghui Zhao, Yangyang Fan, Huimin Wu,\* and Jiu-an Lv\*

Creating high-speed soft actuators will have broad engineering and technological applications. Snapping provides a power-amplified mechanism to achieve rapid movements in soft actuators that typically show slow movements. However, precise control of snapping dynamics (e.g., speed and direction of launching or jumping) remains a daunting challenge. Here, a bioinspired design principle is presented that harnesses a reconfigurable constraint structure integrated into a photoactive liquid crystal elastomer actuator to enable tunable and programmable control over its snapping dynamics. By reconfiguring constrained fin-array-shaped structure, the snapping dynamics of the structured actuator, such as launching or jumping angle and height, motion speed, and release force can be on-demand tuned, thus enabling controllable catapult motion and programmable jumping. Moreover, the structured actuators exhibit a unique combination of ultrafast moving speed (up to  $2.5 \text{ m s}^{-1}$  in launching and  $0.22 \text{ m s}^{-1}$  in jumping), powerful ejection (long ejection distance of  $\approx 20 \text{ cm}$ ,  $35 \text{ mg}$  ball), and high jumping height ( $\approx 8 \text{ cm}$ , 40 times body lengths), which few other soft actuators can achieve. This study provides a new universal design paradigm for realizing controllable rapid movements and high-power motions in soft matter, which are useful for building high-performance soft robotics and actuation devices.

ubiquitously shown by living organisms, in which mechanical instability enables a bistable structure to rapidly switch from one stabilized form to another via releasing pre-stored elastic energy, allows living organisms whose usual display slow natural rates of deformation/motion to gain high-speed and powerful actions.<sup>[4]</sup> For example, elaterid beetles employ a hinge mechanism that amplifies muscle power, thus achieving the fast launch maneuver.<sup>[5,6]</sup> Larvae of *Asphondylia* can accumulate sufficient energy via bending its body and release the energy to achieve a high jump for evading predators.<sup>[7,8]</sup> The leaves of Venus flytrap can rapidly close up within one-tenth of a second to catch insects.<sup>[9,10]</sup> Mantis shrimp can make use of a saddle-shaped exoskeletal spring mechanism to produce an extremely fast and powerful punch to smash shells and impale fish.<sup>[11,12]</sup> All these fast-snapping behaviors play a significant role in the survival of living organisms, which allow those slow-moving species to efficiently enable rapid

hunting, escaping, spreading seeds,<sup>[13,14]</sup> and overcoming large obstacles, etc.

To realize rapid movements in synthetic materials, scientists and engineers have developed stimuli-responsive soft materials systems of composite elastomers,<sup>[15–21]</sup> gels,<sup>[22–27]</sup> shape memory polymers,<sup>[28–30]</sup> or liquid crystal polymers,<sup>[31–39]</sup> which can perform high-speed shape-changing by taking advantage of snapping mechanics that allows for efficient storing, releasing, and converting elastic energy to kinetic energy. For example, Crosby et al. made use of transient shape changes of a polymer gel to induce snap-through buckling that endows the gel with autonomous snapping and jumping motions.<sup>[26]</sup> Wu and his colleagues created a bistable domal hydrogel structure that allows for fast and reversible snapping actions driven by electric field.<sup>[27]</sup> White's group demonstrated that light-triggered snap-through of bistable arches enables giant enhancement in actuation rates and powers of liquid crystal network.<sup>[37]</sup> Zeng et al. report an optical-controlling latching strategy to modulate the launching dynamics of a LCE actuator, light-induced crystal-to-liquid phase transition of an LC adhesive was employed as a reversible photomechanical latch to achieve precise regulation of the onset timing and speed of motion of the launching event.<sup>[38]</sup>

## 1. Introduction

Nature offers creative principles and inspirations to devise high-speed soft actuators and robots.<sup>[1–3]</sup> Snapping motions

J. Wang

School of Materials Science and Engineering  
Zhejiang University  
Hangzhou 310027, China

J. Wang, T. Zhao, Y. Fan, H. Wu, J.-a. Lv


Key Laboratory of 3D Micro/Nano Fabrication and Characterization of  
Zhejiang Province  
School of Engineering  
Westlake University

18 Shilongshan Road, Hangzhou, Zhejiang 310024, China

E-mail: wuhuimin@westlake.edu.cn; lvjiuan@westlake.edu.cn

J. Wang, T. Zhao, Y. Fan, H. Wu, J.-a. Lv

Institute of Advanced Technology  
Westlake Institute for Advanced Study  
18 Shilongshan Road, Hangzhou, Zhejiang 310024, China

 The ORCID identification number(s) for the author(s) of this article can be found under <https://doi.org/10.1002/adfm.202209798>.

DOI: 10.1002/adfm.202209798



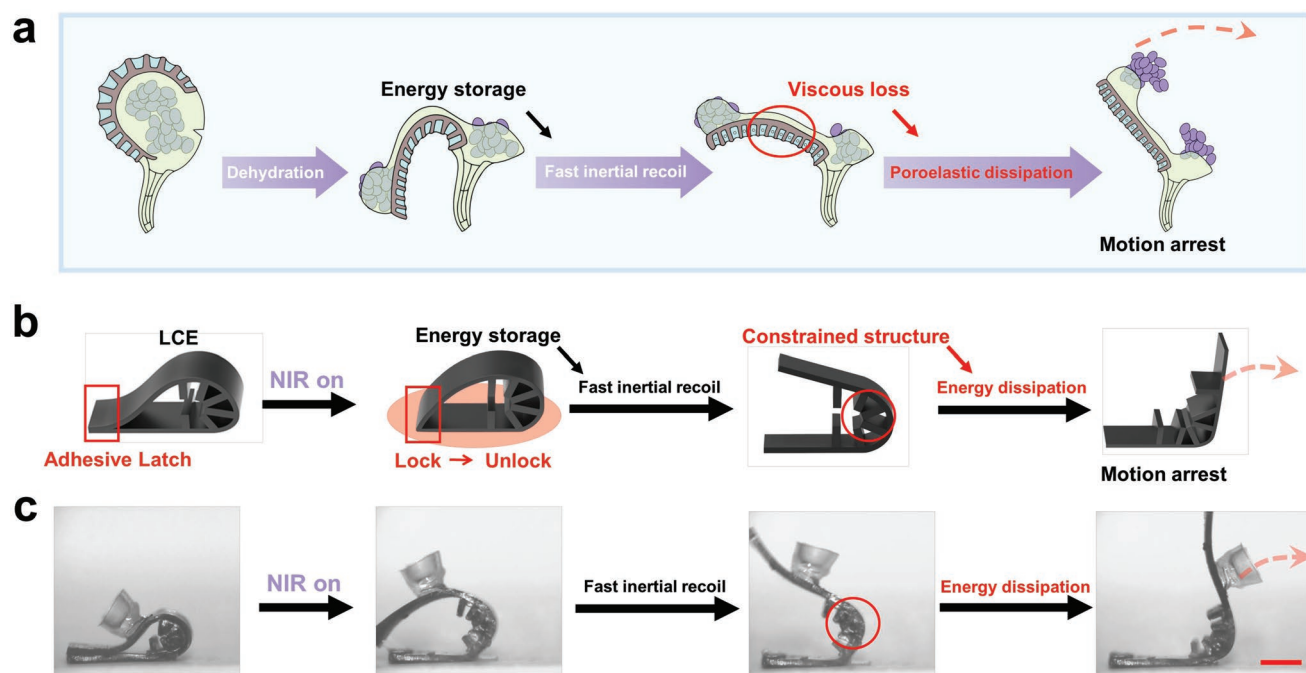


**Figure 1.** Bioinspired design principle based on structural-constraint-based snapping mechanism of fern sporangia. a) Unique ejection mechanism of fern sporangium (*Polypodium aureum*).<sup>[41]</sup> b) Schematic diagram of light-controlled motion arrest launcher with bioinspired constrained fin-array-shaped structure. c) Experimental photograph showing light-controlled LCE actuator with controllable snapping motions corresponding to (b). Scale bar in (c) is 2 mm.

For all these snapping material systems, however, once the construction of snappers is completed, their snapping dynamics would be fixed to be constant and depend on the prescribed bending curvature of the material, which only allows for limited adjustment of the response rate in a small range through changing the intensity of external stimuli. Whereas, for real engineering applications, versatile high-speed soft actuators with tunable snapping dynamics, which can adapt to diverse applications with varying requirements, are preferred.<sup>[40]</sup> Therefore, an effective design strategy capable of tuning snapping dynamics (e.g., magnitude and directionality) is highly needed to develop sophisticated high-speed soft actuators.

Looking to nature for the design strategy of tunable snapping dynamics, we noticed the snapping plants that show high-speed dispersal of seeds or spores through ejection. An expressive example is the physical-constraint-regulated catapult of fern sporangia. When dehydrating, the sporangia open and store elastic energy and then release the stored elastic energy to drive a fast closure action to eject its spores (Figure 1a). Unlike man-made catapults that need a crossbar to arrest the arm's motion midway for the directional control of projectile motion (without the crossbar, projectiles would be launched into the ground), sporangia leverage their accordion-like structure to generate physical constraint to enable controllable ejection instead of using a crossbar, which arises from two different time scale actuations during its closure process. The first is the fast recoil motion after the release of the elastic energy stored in the dehydrated and opened sporangia, and the second is slow motion results from poroelastic dissipation, which can prevent the sporangia's fast recoil, leading to ejecting spores via the inertia.<sup>[41]</sup> The controllable snapping dynamics shown by sporangia can

be achieved by its reconfigurable physical constraint of accordion-like structure.

Inspired by this natural design principle, we have developed a bioinspired design strategy integrating and leveraging reconfigurable structural constraints into a LCE actuator to enable tunable magnitude and directionality in its snapping dynamics, which allows for controllable and programmable high-speed actuation. Reconfigured fin-array-shaped constrained structure inspired by fern sporangia can not only alter the local bending stiffness of the actuator and thus change its stored elastic energy, but also endow it with the capability to manipulate degrees of motion arrest. We demonstrate that the structured LCE actuators can be acted as light-controlled catapults and jumping robots, which exhibit controlled launching and jumping behaviors with well-defined speeds and directions in 3D space.

## 2. Results and Discussion

### 2.1. Structural Design of High-Speed Actuators

Inspired by the structural-constraint-based snapping mechanism of fern sporangia, we devised a new ultrafast actuator with a reconfigurable fin-array-shaped constraint structure as shown in Figure 1b,c, its fabrication method is shown in Figure 2a (see details of the preparation in the Experimental Section), the number of fins and the distance between them can be adjusted according to practical requirements (Figure S2, Supporting Information). In this snapping system, the fin-array-shaped structure provides the physical constraint; a photoactive LCE

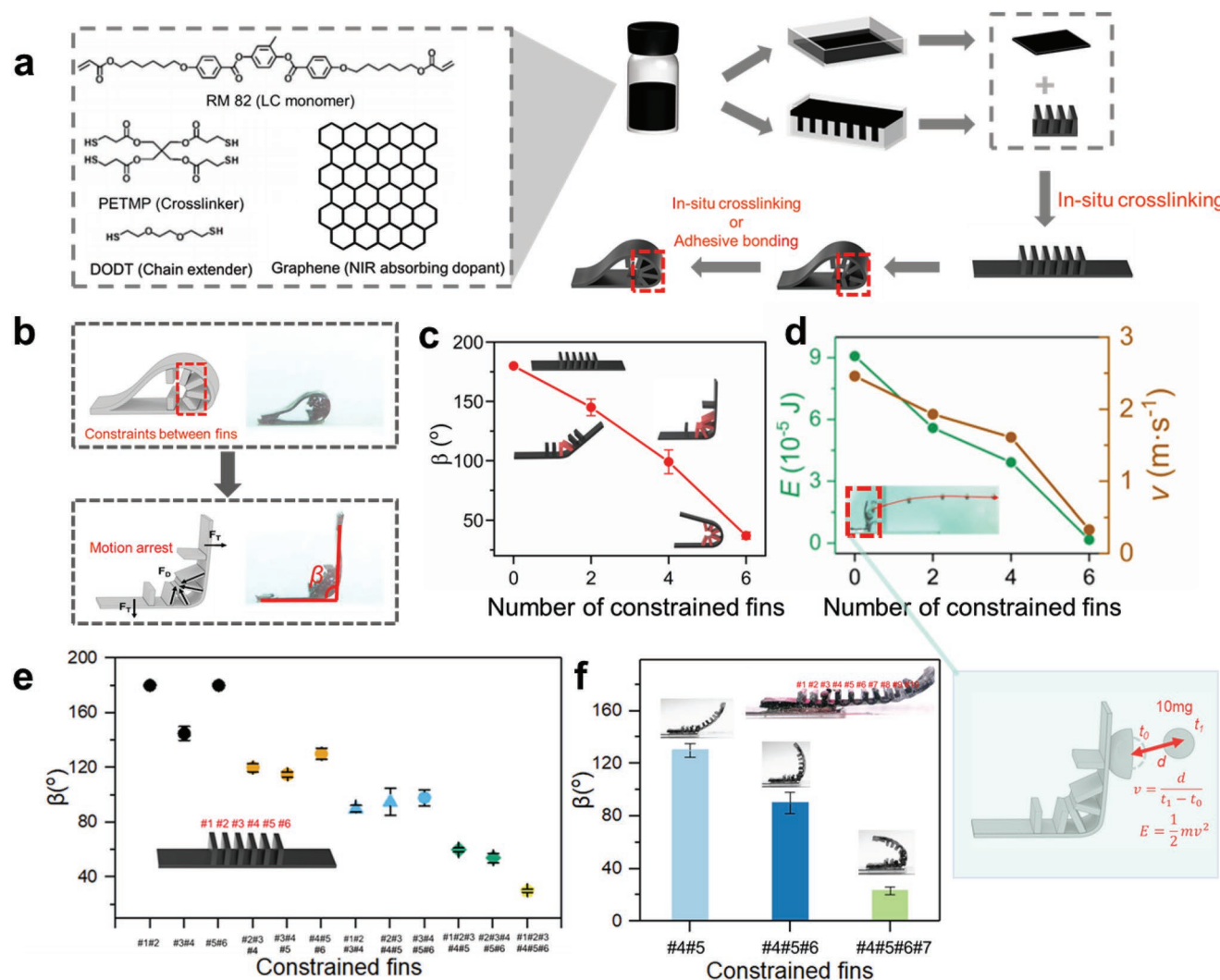


**Figure 2.** Controllable snapping behaviors regulated by reconfigurable constrained structures. a) Synthesis of the LCE ultrafast soft actuator. b) Motion arrest of high-speed actuator. c) Maximum opening angle of LCE actuator with different numbers of constrained fins. d) Light-induced elastic energy  $E$  and launching velocity  $v$  of LCE actuator with different numbers of constrained fins. Inset: Schematic drawing of the light-induced launching process of LCE actuator.  $E$ , elastic energy;  $d$ , Projectile moving distance;  $m$ , Projectile weight;  $v$ , launching velocity. e) The maximum opening angle of the actuator possessed constrained fins with different positions and numbers (Number of fins: 6). f) The maximum opening angle of constrained fins with different positions and numbers (Number of fins: 10). The error bars indicate the standard deviation for  $n = 3$  measurements.

is responsible for the pre-storage and transfer of elastic energy under near-infrared (NIR) irradiation; a temperature-sensitive acrylate adhesive serves as a reversible latch.

The snapping process is schematically and experimentally illustrated in Figure 2b (left) and Figure 2b (right), respectively. After the photo-driven unlock of the mechanical connection (see Figure 3c for more information), the energy stored in the actuator bursts instantaneously, resulting in the ultrafast opening motion of the actuator, and causing an instantaneous external impact force  $F_r$ . The constrained fins would produce inward tension  $F_D$  to stop the fast opening motion of the snapping actuator, leading it to open at a well-defined angle. After removing the NIR light, the actuator would return to the original folding shape and reconnect the latch due to the shape recovery and reversibility of the adhesive, which restarts when the light was irradiated again. Figure 2c shows the maximum opening angle that the LCE

actuator can achieve under a large NIR light intensity with different numbers of constrained fins. For the convenience of characterization, we tested the snapping behavior of actuators with intermediate symmetric 0, 2, 4, and 6 constrained fins. When all the fins were not constrained, the actuator can be opened to the maximum (180°). When the whole six fins were bonded together and constrained, the actuator could only be opened at ≈40°. To evaluate the controllability of the LCE actuator during the snapping process, the effect of the constrained fins on the motion state of the projectile (10 mg) was investigated. First, as shown in Figure 2d, Figure S10, and Movie S1 (Supporting Information), the initial velocity  $v$  and kinetic energy  $E$  of the projectile were calculated by recording the shooting angle and landing point frame by frame with an ultra-high-speed camera. When all the fins were not constrained, the calculated  $v$  and  $E$  are as high as ≈2.46 m s<sup>-1</sup> and  $9.08 \times 10^{-5}$  J. When the whole six

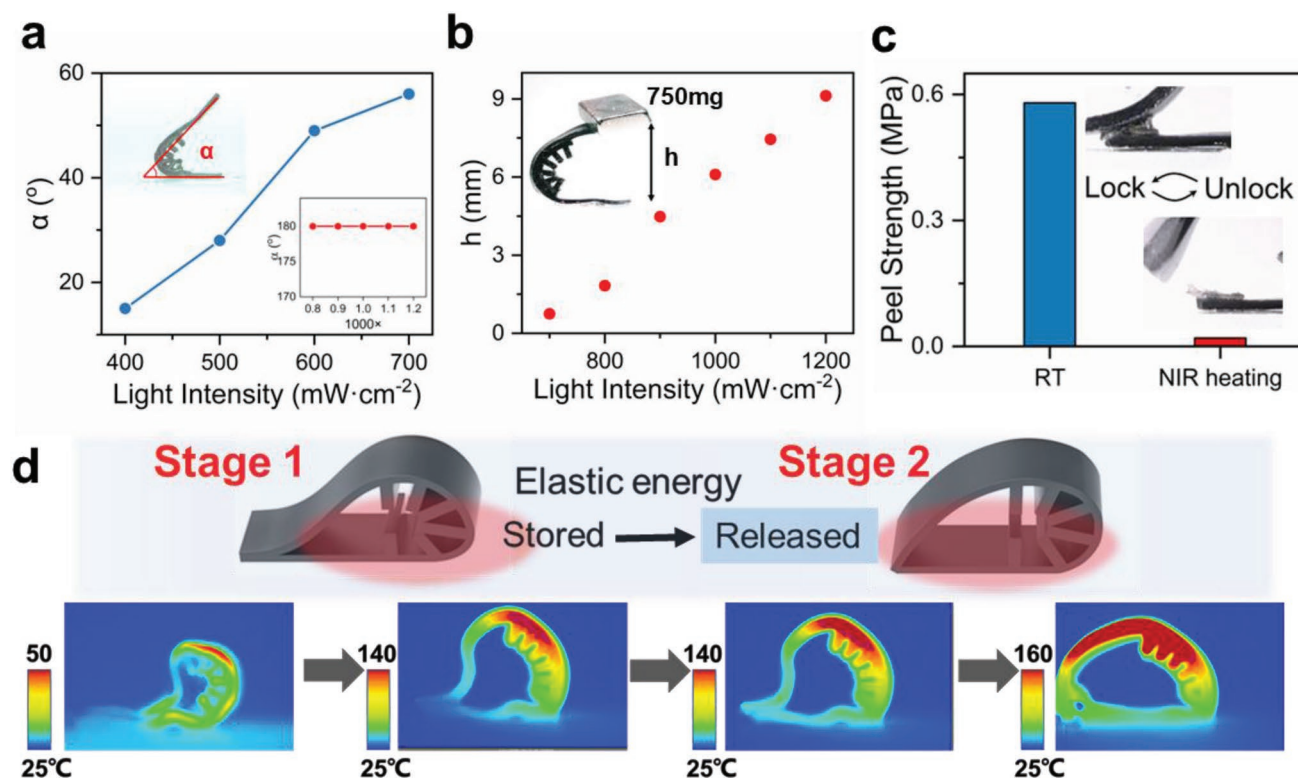


**Figure 3.** Controllable snapping motions of the LCE snapper. a) Opening angle of a folded LCE under different light intensities. b) A folded LCE lifting an object of 750 mg, 20× body weight (BW) under different light intensities. c) Mechanical test of the adhesive force under room temperature and NIR heating for 5 s ( $I \approx 1.2 \text{ W cm}^{-2}$ ). d) Unlocking process of the bonded area and thermal imaging shows the temperature distribution of LCE actuator in different stages.

fins were constrained, the  $\nu$  and  $E$  of the projectile decrease to  $0.33 \text{ m s}^{-1}$  and  $0.17 \times 10^{-5} \text{ J}$ , which indicates that the constrained fins can control the snapping process by consuming the stored energy, suggesting the number of constrained fins is an important parameter for a controllable light-driven snapping process owing to its excellent energy consumption ability. Moreover, the snapping motion of the actuator can be tunably and programmably controlled not only through changing the number and position of the constrained fins (Figure 2e; Figure S3, Supporting Information), but also by changing the total number of fins in the fin-array-shaped structure (Figure 2f; Figure S4, Supporting Information). Therefore, ultrafast actuators with different degrees of motion suspension can be prepared, which proves the concept of the light-driven ultrafast actuator with controllable snapping behavior.

## 2.2. NIR Light-Controlled LCE Part and Latch

A photoactive LCE and a temperature-responsive acrylate adhesive are responsible for energy storage and controllable release, respectively. The LCE in this study exhibits a relatively low glass transition temperature of  $\approx -7.2^\circ\text{C}$  and a nematic–isotropic transition temperature of  $\approx 90.7^\circ\text{C}$  (Figure S5, Supporting Information). Upon NIR light irradiation, the surface temperature of the actuator can rapidly increase above isotropic transition temperature in seconds, leading the LCE to quickly undergo

ordered-to-disordered transition. The decrease in liquid crystalline ordering gives rise to a contraction at the folded part of the irradiated soft actuator, resulting in an obvious reversible opening deformation. Figure 3a illustrates the light-driven opening behavior of a soft actuator under NIR light irradiation, and the corresponding infrared thermal images (Figure S7, Supporting Information) indicate the photo-induced temperature change of the irradiated LCE actuator. The performance of the soft actuator was investigated under different NIR light intensities. With the increase of light intensity, the surface temperature and opening angle of the soft actuator increased. When the light intensity increases to  $800 \text{ mW cm}^{-2}$ , the LCE soft actuator can exhibit a maximum opening angle of  $180^\circ$  owing to the increase in the irradiated area. By transforming light energy into mechanical output, the large light-induced stress of the actuator can allow heavy mass lifting, up to tens of times of its own body. To measure the photoinduced force of the LCE soft actuator, we measured the height of lifting heavy mass by the actuator upon 808 nm NIR light irradiation with different intensities. The driving force originates from the mechanical opening of the soft actuator, which is almost proportional to the light intensity (Figure 3b).

The acrylate adhesive is used as the controllable latch for energy release. At room temperature (RT), the adhesive can provide a firm connection between the two ends overlapping. The bonding strength of the adhesive quickly decreases above  $110^\circ\text{C}$  and the mechanical connection is unlocked. Such transition is



reversible and the connection can recover when cooling to RT (Figure S8, Supporting Information). According to Figure 3c, the peel strength of adhesive at RT is up to 0.58 MPa and then drops to  $\approx 0.02$  MPa after NIR heating for 5 s. This offers an effective switch for locking/unlocking the launching mechanics, which the whole launching process can be controlled by NIR light. As shown in Figure 3d, the launching process is divided into two stages. In stage one, only the part other than the latch of the actuator is driven by NIR light. When the LCE part is heated until the curvature no longer changes, stage two can be carried out. Moving the NIR light spot until all parts of the actuator can be heated by light, and the temperature of the overlapping part rises above the unlocking temperature of the latch, followed by the release of stored energy and instant movement of LCE, yielding control over the whole launching process. Together with the reversibility of folding-oriented LCE deformation, it provides a basis for the good repeatability of the LCE ultrafast actuator.

### 2.3. LCE Catapult with Controllable Snapping Motions

Since the LCE actuator can simultaneously provide ultrafast snapping motion and motion arrest, we further demonstrate

its ability to export mechanical work as a catapult without using the crossbar (Figure 4a). To evaluate the controllability of the LCE catapult during the shooting process, the effect of the constrained fins of the LCE catapult on the motion state of the projectile was investigated. When the capture motion is stopped, the opening angle of the actuator is varied, resulting in different shooting heights and ejection distances of the ball (Figure 4b,c). When the four fins fit together, the snap motion would arrest when the opening angle is  $\approx 100^\circ$ , and the object can be projected in the corresponding direction. However, when all six fins are constrained, the opening motion can be immediately arrested, and the kinetic energy of the projectile is not enough to make it produce a large motion. Therefore, as the number of constrained fins increases, the initial shooting height and ejection distance of the ball increase first and then decrease, reaching the maximum (13 mm and 20 cm) when the number of constrained fins is 4. As shown in Figure 4d and Movie S2 (Supporting Information), the catapult can throw a 35 mg iron ball into a basket at a distance of 12 cm and a height of 2 cm accurately within 0.24 s. For the ultrafast actuator prepared in this study, the control of the stored elastic energy releasing is not based on adhesive, but on the special fin-array-shaped structure. Therefore, a single actuator can carry out

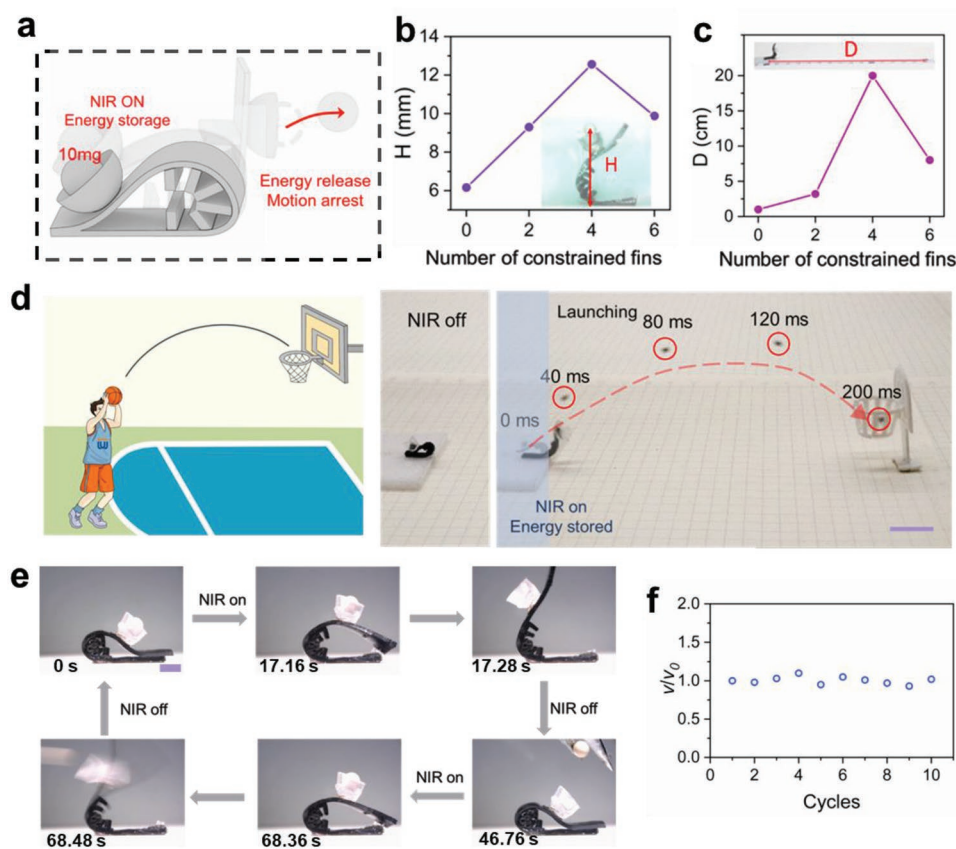


**Figure 4.** Light-controlled catapult. a) Light-induced launching process of a motion-arrest LCE catapult. b) The projectile (10 mg) height of LCE catapult with different numbers of constrained fins. c) The projectile (35 mg) launch distance  $D$  of LCE catapult with different numbers of constrained fins. d) Photograph of the LCE catapult shooting a ball (35 mg) into a basket at a distance of 12 cm and height of 2 cm under NIR light stimulation. Multiple photographs during the throwing process showed the flying path of the ball. Scale bar is 1 cm. Illumination conditions are  $1.2 \text{ W cm}^{-2}$ . e) Reversibility of the light-controlled launching action. Scale bar is 2 mm. f) The ratio between the velocity  $v$  of the projectile after each launching cycle and the velocity of the first launching event ( $v_0$ ). The number of constrained fins in (d), (e), and (f) is 4.

stable and repeated snapping motion without external intervention (Figure 4e; Movie S3, Supporting Information), such as exemplified by monitoring the launching speed over multiple events within the same actuator under identical illumination conditions (Figure 4f).

## 2.4. LCE Jumping Robot with Controllable Snapping Motions

With the help of the suddenly released kinetic energy and the impact energy on the ground, our high-speed actuator can work as a jumping robot to exert a jumping action of somersault (Figure 5a–c). A video of the whole jumping process is given in Movie S4 (Supporting Information). As shown in Figure 5a and Movie S5 (Supporting Information), the robot can jump up to a height of  $\approx 8$  cm (more than 40 times its body length) and an initial speed of  $\approx 22$  cm s<sup>-1</sup> without constrained fins. Like the LCE catapult, the jumping motion can be regulated by the constrained-fins structure. With the change in the number of constrained fins, the jumping height

and speed can be well defined (Figure 5d; Figure S11, Supporting Information).

For real engineering applications, it is important to sustain jumping with heavy loading.<sup>[42]</sup> Our powerful jumper can not only carry cargos 0.5 times heavier than its own weight to generate jumping motion (Figure 5e), but also be combined with a LCE catapult to cross multi-level obstacles. Taking advantage of the tailorable photoresponsiveness of different dyes, we develop soft LCE actuators with multi-wavelength selectivity (Figure S9, Supporting Information). Light-driven LCE jumping robot and catapult based on two different dyes are fabricated. LCE jumping robot and catapult are selectively activated to light irradiation with 520 and 808 nm, respectively. Under the irradiation of 520 nm green light, the jumping robot selectively undergoes jump motion in the corresponding direction. Similarly, the LCE catapult performs the act of ejection only under the irradiation of 808 nm NIR light. Furthermore, we challenged the multiple soft actuators to relay linear cargo under sequential multi-light irradiations. As schematically illustrated in Figure 5f and Movie S6 (Supporting Information), the green-light-responsive

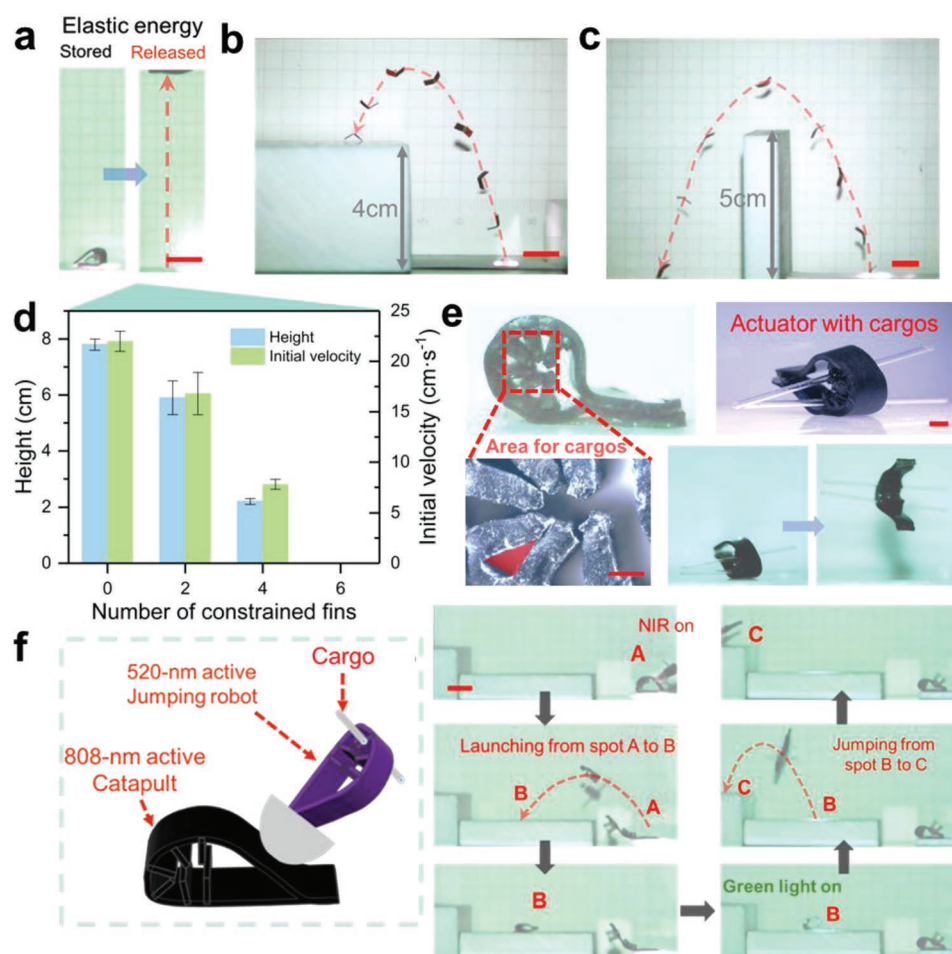


**Figure 5.** Controllable jumping robot. a) Photographs of light-controlled jumping. b) Snapshots of the LCE jumping robot bouncing onto the platform. c) Snapshots of the LCE jumping robot bouncing over the obstacle. d) Jumping height and initial velocity of LCE jumping robot with different numbers of constrained fins. e) The cargos are loaded into the LCE jumping robots. f) The LCE catapult responding to NIR light and the LCE jumping robot responding to green light are combined to relay the cargo. Scale bars in (a), (b), (c) and (f) are 1 cm. Scale bars in (e) are 500  $\mu$ m. Light intensity is 1.2 W cm<sup>-2</sup>.

jumping robot loading linear cargo was placed inside the bowl of the NIR-light-responsive soft catapult. The cargo can be delivered from initial position A to final position C in two steps: i) Ejecting to position B under 808 nm NIR light irradiation; ii) Jumping from position B to position C under 520 nm green light irradiation. These results indicate that the modulation of the wavelength bands of light stimulus can precisely control the multiple snapping motion modes of those soft LCE actuators.

## 2.5. LCE Actuators with Controllable Direction Adjustment

To elucidate the adaptive directional regulation mechanism, we further investigate the light-tracking and self-regulating

snapping process of the soft catapult with the 808 nm NIR light irradiated from three zenith angles. As shown in **Figure 6a** and **Figure S12** (Supporting Information), the LCE soft catapult originally placed in the middle is capable of adaptively responding to the NIR light irradiations from different zenith angles, respectively. The latch part of the actuator could detect the NIR light irradiation, thus causing unlocking of the corresponding position due to localized photo-thermal heating and subsequent shape deformation. when the long axis of the NIR spot is parallel to that of the actuator, both ends of the latch part undergo symmetrically deformation, yielding forward motion. When the tilted NIR spot is used, the latch part experiences large asymmetrical changes, and the area close to the NIR spot will be unlocked first, resulting in the turning of motion direction. As

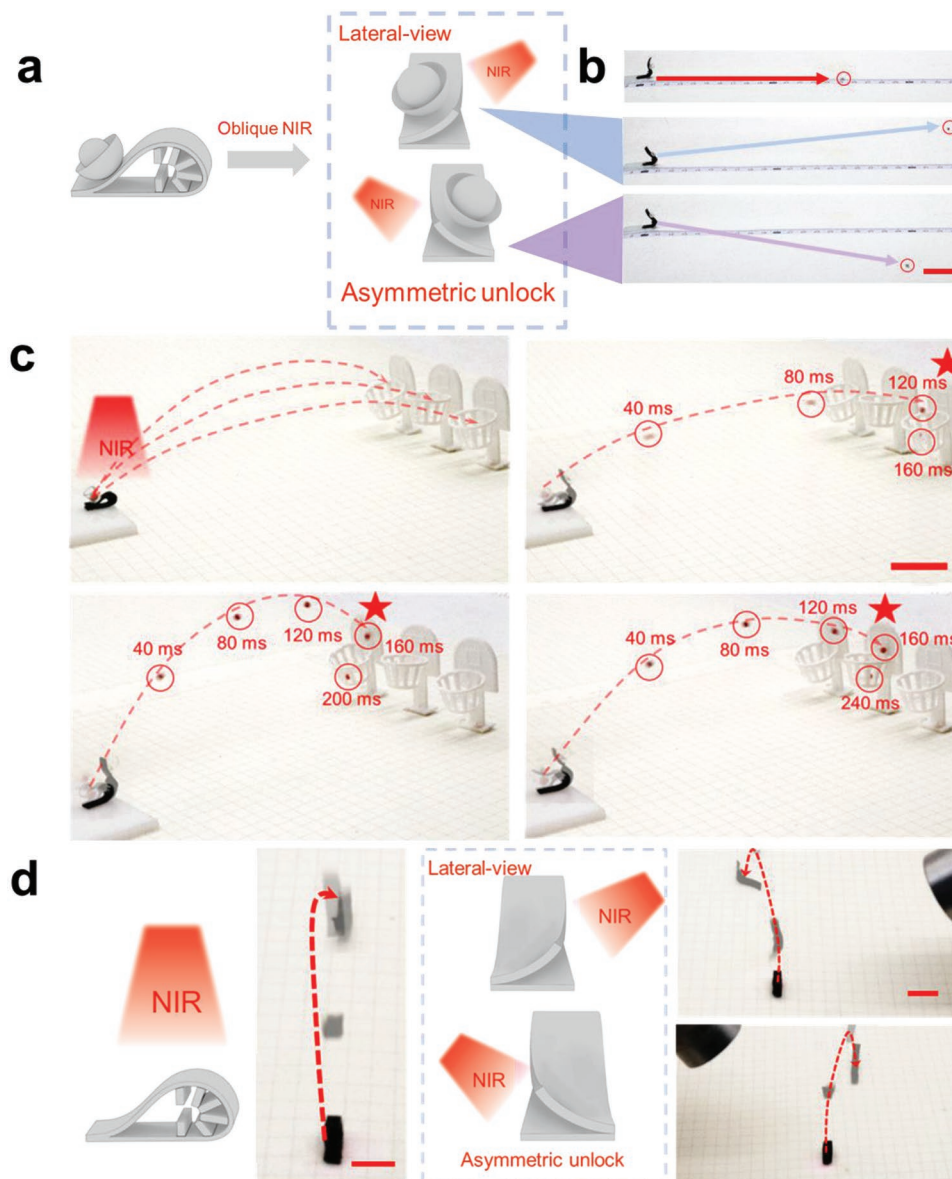


**Figure 6.** Tunable launching direction. a) Asymmetric unlocking of the bonded area through adjusting the NIR light. b) Light-controlled catapult projectiles objects in different directions. c) Photograph of the LCE catapult shooting a ball into three adjacent baskets through adjusting the NIR light. Scale bars in (b) and (c) are 2 cm. d) The light-controlled LCE jumping robot jumps in different directions. Scale bar: 1 cm. Light intensity:  $1.2 \text{ W cm}^{-2}$ .



shown in Figure 6b, the LCE catapult can project an iron ball weighing 35 mg in three directions. In addition, the catapult can throw the ball into three adjacent baskets by modulating NIR light spots (Figure 6c; Movie S7, Supporting Information). Based on the same steering strategy, we also can flexibly steer the jumping robot jump along the desired pathway on demand. As shown in Figure 6d and Movie S8 (Supporting Information), the jumping robot can also flexibly turn in three desired directions. The multidirectional controllability of such LCE soft actuators is of paramount significance for the development of adaptive intelligent soft robotics, active locomotion-controlled soft actuators, and sophisticated high-speed soft devices.

### 3. Conclusion

In summary, we exhibit a versatile bioinspired strategy to devise high-speed soft actuators with tunable and programmable snapping dynamics via reconfigurable structural constraints. The constrained accordion-like architecture in fern sporangia provides the inspiration for the creation of ultrafast soft actuators with constrained fin-array-shaped structures that are leveraged to regulate snapping behaviors. By modulating the constrained-fins structure, we precisely control the snapping-induced motion behaviors in 3D space and demonstrate their promising applications as contactless and remote-controlled catapults and jumping robots with controllable snapping behaviors. Our design principle based on reconfigurable constraint structures could be extended to other soft active systems to endow them with controllable ultrafast dynamics, offering a feasible and effective reconfigurable-structure-based approach to achieving the tunability of snapping dynamics for high-speed soft actuators.

### 4. Experimental Section

**Materials:** RM82 (1,4-bis-[4-(6-acryloyloxyhexyloxy)benzoyloxy]-2-methylbenzene) was purchased from Shijiazhuang Yesheng Chemical Technology Co., Ltd. The acrylate adhesive was purchased from Wuhan zhenfuhui e-commerce Co., Ltd. DODT (3,6-dioxo-1,8-octanedithiol), pentaerythritol tetrakis (3-mercaptopropionate) (PETMP), dipropylamine (DPA, 99%), and graphene were obtained from TCI. All chemicals were used as received.

**Fabrication of LCE Snapping Actuator with Fin-Array-Shaped Structure:** The mixture was formulated with 1.67:1 molar ratio of RM82 and DODT, 3:1 molar ratio of DODT:PETMP, and 2 wt.% graphenes. Thiol groups and acrylate groups were equimolar. The mixture was dissolved in chloroform. After ultrasonic dispersion of 4 h, a catalytic amount of DPA was added to the solution. The mixture containing 200 mg RM82 was transferred into a custom-made Teflon mold (3 cm × 1.5 cm × 0.2 cm) quickly. The pre-crosslinking LCE film formed after 2 h at room temperature. At the same time, the mixture containing 100 mg RM82 was dropped on to a mold with continuous concaves (Figure S1, Supporting Information, Concave dimensions: 10 × 1.5 × 0.7 mm<sup>-3</sup>. Concave spacing: 0.7 mm) to prepare fin-array-shaped structure, which was assembled on LCE film by in situ cross-linking method. Following the above preparation, the weakly cross-linked LCE film with a fin-array-shaped structure was folded and maintained for 24 h to complete the cross-linking reaction and fix the orientation of the structured LCE film.

**Characterization:** The surface temperature of the actuator before and after 808 nm NIR irradiation was measured by an infrared thermometer (A665sc, FLIR). Eight hundred eight nanometers NIR light was generated

by a laser source (MDL-H-808-5 W, Changchun New Industries Optoelectronics Technology Co., Ltd). Five hundred twenty nanometers green light was produced by commercial laser pointers (Beijing Huisite Technology Co., Ltd). The laser intensity was monitored by a laser power meter (TP100, Changchun New Industries Optoelectronics Technology Co., Ltd). 2D WAXD experiments were carried out on a Bruker D8 Venture diffractometer with a PHOTON III detector with an incoatec microfocus source (Cu K $\alpha$ ,  $\lambda$  = 1.5418 Å) equipped with an Oxford 800 Plus liquid nitrogen vapor cooling device. The photographs and videos of the NIR-light-driven experiments were recorded by a super-resolution digital microscope (Keyence, VHX-6000) or a digital camera (Canon, EOS 80D(W)). The videos of snapping motion were recorded by a high-speed microscope VW-9000. Peel forces of the acrylate adhesive were measured using a tensile machine of Instron 5943.

### Supporting Information

Supporting Information is available from the Wiley Online Library or from the author.

### Acknowledgements

This research was supported by National Natural Science Foundation of China (51873197), Natural Science Foundation of Zhejiang Province of China (LR22E030004), 151 Talent Project of Zhejiang Province, and Foundation of Westlake University.

### Conflict of Interest

The authors declare no conflict of interest.

### Data Availability Statement

The data that support the findings of this study are available in the supplementary material of this article.

### Keywords

fin-array-shaped structures, high-speed actuators, photo-induced shape changes, physical constraints, tunable snapping

Received: August 24, 2022

Revised: October 3, 2022

Published online:

- [1] R. Baumgartner, A. Kogler, J. M. Stadlbauer, C. C. Foo, R. Kaltseis, M. Baumgartner, G. Y. Mao, C. Keplinger, S. J. A. Koh, N. Arnold, Z. G. Suo, M. Kaltenbrunner, S. Bauer, *Adv. Sci.* **2020**, 7, 1903391.
- [2] S. Poppinga, T. Masselter, T. Speck, *BioEssays* **2013**, 35, 649.
- [3] Y. Forterre, *J. Exp. Bot.* **2013**, 64, 4745.
- [4] R. Sachse, A. Westermeier, M. Mylo, J. Nadasdi, M. Bischoff, T. Speck, S. Poppinga, *Proc. Natl. Acad. Sci.* **2020**, 117, 16035.
- [5] O. Bolmin, L. H. Wei, A. M. Hazel, A. C. Dunn, A. Wissa, M. Alleyne, *J. Exp. Biol.* **2019**, 222, jeb196683.
- [6] G. Ribak, D. Weihs, *PLoS One* **2011**, 6, e20871.
- [7] D. P. Maitland, *Nature* **1992**, 355, 159.
- [8] G. M. Farley, M. J. Wise, J. S. Harrison, G. P. Sutton, C. Kuo, S. N. Patek, *J. Exp. Biol.* **2019**, 222, jeb201129.

- [9] A. Pandey, D. E. Moulton, D. Vella, D. P. Holmes, *Europhys. Lett.* **2014**, *105*, 24001.
- [10] Y. Forterre, J. M. Skotheim, J. Dumais, L. Mahadevan, *Nature* **2005**, *433*, 421.
- [11] S. N. Patek, W. L. Korff, R. L. Caldwell, *Nature* **2004**, *428*, 819.
- [12] E. Steinhardt, J. Koh, M. H. Rosen, S. N. Patek, R. J. Wood, *Proc. Natl. Acad. Sci.* **2021**, *118*, e2026833.
- [13] D. L. Whitaker, J. Edwards, *Science* **2010**, *329*, 406.
- [14] L. Yafetto, L. Carroll, Y. L. Cui, D. J. Davis, M. W. F. Fischer, A. C. Henterly, J. D. Kessler, H. A. Kilroy, J. B. Shidler, J. L. Stolze-Rybczynski, Z. Sugawara, N. P. Money, *PLoS One* **2008**, *3*, e3237.
- [15] D. Lunni, M. Cianchetti, C. Filippeschi, E. Sinibaldi, B. Mazzolai, *Adv. Mater. Interfaces* **2020**, *7*, 1901310.
- [16] H. Q. Shao, S. Z. Wei, X. Jiang, D. P. Holmes, T. K. Ghosh, *Adv. Funct. Mater.* **2018**, *28*, 1802999.
- [17] X. Wang, G. Y. Mao, J. Ge, M. Drack, G. S. C. Bermúdez, D. Wirthl, R. Illing, T. Kosub, L. Bischoff, C. Wang, J. Fassbender, M. Kaltenbrunner, D. Makarov, *Commun. Mater.* **2020**, *1*, 67.
- [18] A. Pal, D. Goswami, R. V. Martinez, *Adv. Funct. Mater.* **2020**, *30*, 1906603.
- [19] O. Bas, B. Gorissen, S. Luposchainsky, T. Shabab, K. Bertoldi, D. W. Huttmacher, *Multifunct. Mater.* **2021**, *4*, 045001.
- [20] Y. Hu, J. Q. Liu, L. F. Chang, L. L. Yang, A. F. Xu, K. Qi, P. Lu, G. Wu, W. Chen, Y. C. Wu, *Adv. Funct. Mater.* **2017**, *27*, 1704388.
- [21] Y. C. Tang, Y. D. Chi, J. F. Sun, T. H. Huang, O. H. Maghsoudi, A. Spence, J. G. Zhao, H. Su, J. Yin, *Sci. Adv.* **2020**, *6*, 6912.
- [22] H. Lee, C. Xia, N. X. Fang, *Soft Matter* **2010**, *6*, 4342.
- [23] Y. Jiang, L. M. Korpas, J. R. Raney, *Nat. Commun.* **2019**, *10*, 128.
- [24] W. Fan, C. Shan, H. Guo, J. Sang, R. Wang, R. Zheng, K. Sui, Z. Nie, *Sci Adv* **2019**, *5*, eaav7174.
- [25] Q. Zhao, X. Yang, C. Ma, D. Chen, H. Bai, T. Li, W. Yang, T. Xie, *Mater. Horiz.* **2016**, *3*, 422.
- [26] Y. Kim, J. van den Berg, A. J. Crosby, *Nat. Mater.* **2021**, *20*, 1695.
- [27] C. Y. Li, S. Y. Zheng, X. P. Hao, W. Hong, Q. Zheng, Z. L. Wu, *Sci. Adv.* **2022**, *8*, eabm9608.
- [28] T. Chen, O. R. Bilal, K. Shea, C. Daraio, *Proc. Natl. Acad. Sci.* **2018**, *115*, 5698.
- [29] J.-S. Koh, E. Yang, G.-P. Jung, S.-P. Jung, J. H. Son, S.-I. Lee, P. G. Jablonski, R. J. Wood, H.-Y. Kim, K.-J. Cho, *Science* **2015**, *349*, 517.
- [30] Z. Zhakypov, K. Mori, K. Hosoda, J. Paik, *Nature* **2019**, *571*, 381.
- [31] T. H. Zhao, W. Fang, Y. Y. Fan, Z. M. Hu, H. Wu, X. Q. Feng, J. A. Lv, *Adv. Mater. Technol.* **2022**, *3*, 2101660.
- [32] H. Shahsavan, A. Aghakhani, H. Zeng, Y. Guo, Z. S. Davidson, A. Priimagi, M. Sitti, *Proc. Natl. Acad. Sci.* **2020**, *117*, 5125.
- [33] A. S. Kuenstler, Y. Chen, P. Bui, H. Kim, A. DeSimone, L. Jin, R. C. Hayward, *Adv. Mater.* **2020**, *32*, 2000609.
- [34] Z. M. Hu, Y. L. Li, J. A. Lv, *Nat. Commun.* **2021**, *12*, 3211.
- [35] J. Jeon, J.-C. Choi, H. Lee, W. Cho, K. Lee, J. G. Kim, J.-W. Lee, K.-I. Joo, M. Cho, H.-R. Kim, J. J. Wie, *Mater. Today* **2021**, *49*, 97.
- [36] C. Y. Ahn, X. D. Liang, S. Q. Cai, *Adv. Mater. Technol.* **2019**, *4*, 1900185.
- [37] M. R. Shankar, M. L. Smith, V. P. Tondiglia, K. M. Lee, M. E. McConney, D. H. Wang, L. S. Tan, T. J. White, *Proc. Natl. Acad. Sci.* **2013**, *110*, 18792.
- [38] H. S. Guo, A. Priimagi, H. Zeng, *Adv. Funct. Mater.* **2022**, *32*, 2108919.
- [39] Y. Zhao, Y. Chi, Y. Hong, Y. Li, S. Yang, J. Yin, *Proc. Natl. Acad. Sci.* **2022**, *119*, e2200265119.
- [40] I. Apsite, S. Salehi, L. Ionov, *Chem. Rev.* **2022**, *122*, 1349.
- [41] X. Noblin, N. O. Rojas, J. Westbrook, C. Llorens, M. Argentina, J. Dumais, *Science* **2012**, *335*, 1322.
- [42] M. Li, A. Pal, A. Aghakhani, A. Pena-Francesch, M. Sitti, *Nat. Rev. Mater.* **2022**, *7*, 235.